Spray patternation of a multi-hole injector utilizing planar line-of-sight extinction tomography

S. E. Parrish* and R. J. Zink
General Motors R&D
30500 Mound Road
Warren, MI 48090-9055 USA

Y. Sivathanu and J. Lim
En'Urga Inc.
1291A Cumberland Ave.
West Lafayette, IN 47906

Abstract

Spray characteristics of a multi-hole injector intended for use in direct-injection gasoline engines have been evaluated for a variety of operating conditions including those that promote flash boiling. Planar line-of-sight extinction tomography was employed to evaluate spray patterns to determine the influence of ambient pressure and temperature and fuel pressure and temperature on spray structure. Under severe flash boiling conditions, sprays were found to collapse and change shape significantly.

*Corresponding author

Introduction

It is well known that spray characteristics are of vital importance to the fuel economy and emissions of direct-injection gasoline engines [1, 2]. The literature is extensive in the area of spray characterization of injectors intended for use in direct-injected gasoline engines [3-5]. These engines can operate with early and late injection timings. Early injection is employed to promote homogeneous conditions at the time of ignition where as late injection is employed to promote stratified conditions at the time of ignition.

In the case of early injection, injection occurs during the intake stroke and cylinder pressures can be well below atmospheric pressure depending on the amount of throttling that is being utilized. In addition, due to the fuel injector being mounted directly in the cylinder head, injector temperatures, and consequently fuel temperatures, are close to that of the engine coolant. The combination of these low cylinder pressures and high fuel temperatures can superheat the fuel and promote rapid phase change during the injection event. The effects of this phenomenon, commonly referred to as flash boiling, on resulting spray characteristics were of interest in this investigation. Although several have studied these effects utilizing swirl type injectors [6-8], much less has been published related to multi-hole injectors [9,10], which is the injector type evaluated here.

In the case of late injection, injection occurs during the compression stroke and cylinder pressures and temperatures are high due to compression of the intake charge. Multi-hole injectors are of interest because their sprays tend to maintain their shape when exposed to high ambient pressures. Additionally they offer considerable flexibility in fuel placement.

Planar line-of-sight extension tomography was the diagnostic employed to determine the influence of ambient pressure and temperature and fuel pressure and temperature on spray structure. In addition to spray patternation, measurements of included spray angle are presented. The motivation for this work was to improve understanding of multi-hole injector spray characteristics under various operating conditions. The data generated should be of interest to combustion system engineers to assist in combustion system development and to computational modelers for model validation. An ancillary objective of this work was to determine the effectiveness of line-of-sight extinction tomography as a research and development tool for characterizing dense, high velocity, transient sprays.

Experiment Details

The injector used in this investigation was an 8-hole, VCO (valve covered orifice) style injector with a nominal included spray angle of 60 degrees. A coolant jacket surrounding the injector mount was used to control the injector temperature. The fuel temperature was assumed to be equal to the coolant temperature and was set to 20º C to mimic cold conditions and 90º C to mimic fully warmed up conditions. Two injection pressures, 10 MPa and 20 MPa, were investigated and maintained using a nitrogen charged accumulator. The injected mass was fixed at 10 mg, corresponding to injection durations of 0.95 ms and 0.65 ms for the 10 and 20 MPa fuel pressures, respectively. Indolene was chosen as the test fluid due to its realistic multi-component composition.

Experiments were conducted in a pressure vessel that allowed measurements to be performed above and below atmospheric pressure. Ambient pressures ranging from 40 kPa to 1000 kPa were investigated. A continuous flow of nitrogen gas passed through the vessel to provide evacuation of the injected mass. The gas temperature within the vessel ranged from 300° K to 500° K.

Planar line-of-sight extinction data was obtained using a SETscan AP400 optical patternator from En'Urga Inc. The instrument was capable of obtaining time-resolved planar line-of-sight extinction measurements from two planes separated by a fixed distance of 10 mm. The instrument consisted of a transmitter and receiver. The transmitter emitted two planes of laser light each approximately 100 mm wide and 0.6 mm in thickness. The receiver collected the planar line-of-sight extinction data utilizing two line detector arrays each having 512 elements. The transmitter and receiver were positioned on opposite sides of the vessel with the measurement planes located at 30 and 40 mm from the injector tip.

To perform tomography more than one line-of-sight is required, this was achieved by rotating the injector about its axis in 22.5° increments providing a total of eight views. Measurements of 25 injection events were utilized to calculate the average planar line-of-sight extinction at each angular position. The resulting data was then deconvolved using a maximum likelihood deconvolution scheme [11,12]. The end result of the deconvolution process is surface area per unit volume. An example showing average planar line-of-sight extinction measurements and the resulting surface area density contour is depicted in Figure 1.

Data was acquired at a rate of 1 kHz with an integration time of approximately 1 ms. Due to the short injection durations and high speeds, only the first few frames of data were of interest. As an example, Figure 2 shows spray patternation results for the first 3 ms for both measurement planes at a given condition. The times are referenced from the electronic trigger signal sent to the injector driver. It should be noted that there was a delay of approximately 0.3 ms from this reference before the injector opened and started to emit spray. Additionally, it takes some amount of time for the leading edge of the spray to penetrate to the mea-

surement planes. This time is dependent on the operating condition. Therefore, in the case of the first ms frame, spray was present only for some fraction of the 1 ms integration time and corresponds primarily to the leading edge of the spray. Eight fairly symmetric and distinct spray plumes are easily identified. As expected, the spray patterns associated with the 40 mm plane are larger than those of the 30 mm plane due to expansion of the spray in the radial direction. In the case of the 2 ms frames, the spray pattern in the 40 mm plane continues to exhibit distinct individual plumes whereas in the 30 mm plane, individual plumes are difficult to identify. This loss of structure is associated with the presence of the trailing edge of the spray reaching the 30 mm plane. Both measurement planes show little structure and exhibit only low level extinction in the 3 ms frames. This is due to the spray passing through the planes and leaving slow moving residual droplets.

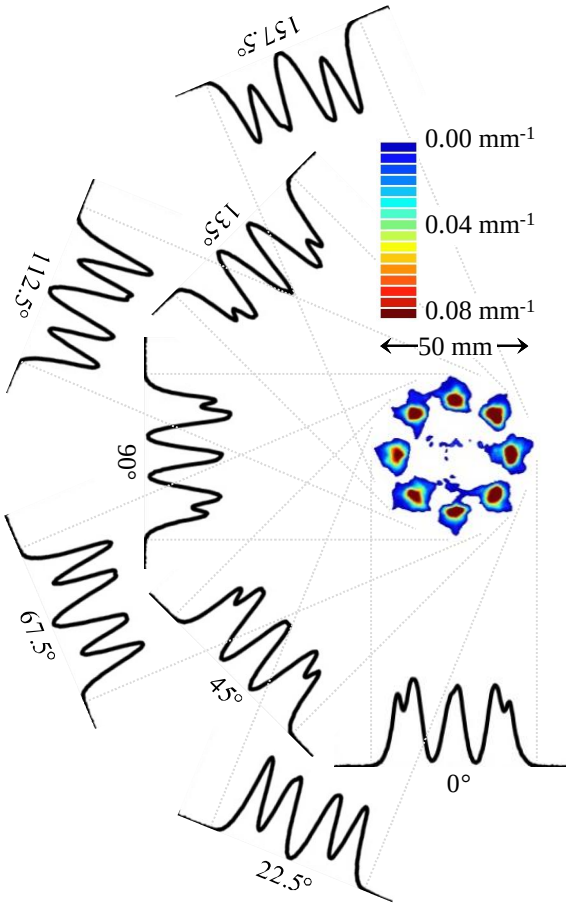

Figure 1. Depiction of planar line-of-sight extinction tomography utilizing eight views. P_{fuel} = 10 MPa, T_{fuel} = 20° C, $P_{ambient}$ = 101 kPa, $T_{ambient}$ = 300° K.

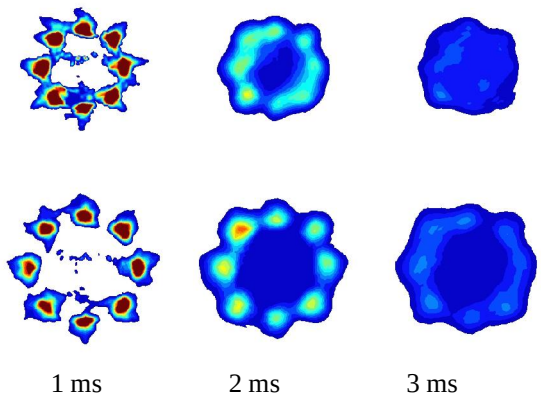

Figure 2. Time resolved patternation. The top row corresponds to the 30 mm plane while the bottom row corresponds to the 40 mm plane. P_{fuel} = 10 MPa, T_{fuel} = 20° C, $P_{ambient}$ = 101 kPa, $T_{ambient}$ = 300° K.

Results and Discussion

Spray Patterns - Figures A.1 through A.6 show the spray patternation results for the conditions investigated. For brevity, only data from the 40 mm measurement plane is shown. Trends were similar for both measurement planes but more clearly resolved in the 40 mm plane. In each figure, the left set of patterns corresponds to the 20° C fuel temperature while the right set corresponds to the 90° C fuel temperature. Each row corresponds to a different ambient pressure and each column corresponds to a different measurement time period. Figures A.1, A.2, and A.3 correspond to the 10 MPa fuel pressure with 300° K, 400° K, and 500° K ambient gas temperatures, respectively, while Figures A.4, A.5, and A.6 correspond to the 20 MPa fuel pressure with 300° K, 400° K, and 500° K ambient gas temperatures, respectively. The spatial and surface area density scaling is identical for all cases and is shown in Figure 1.

Influence of High Ambient Pressure - It is apparent that as ambient pressure is increased the appearance of spray diminishes in the 1 ms frame. This is most evident in the 250 kPa to 500 kPa ambient pressure range. Furthermore, in general, the appearance of spray in the 3ms frame becomes more evident with increasing ambient pressure. These trends are not surprising and are due to a reduction in spray penetration resulting in later arrival in the 1 ms frame and longer persistence in the 3 ms frame. Figure 3 quantifies these effects for the 10 MPa fuel pressure with 90º C fuel temperature. Total surface area decreases with an increase in ambient pressure for the 1 ms time period, while it increases for the 3 ms time period. The exceptional point at 1000 kPa ambient pressure and 300° K ambient temperature for the 3 ms frame is due to an excessive loss of penetration.

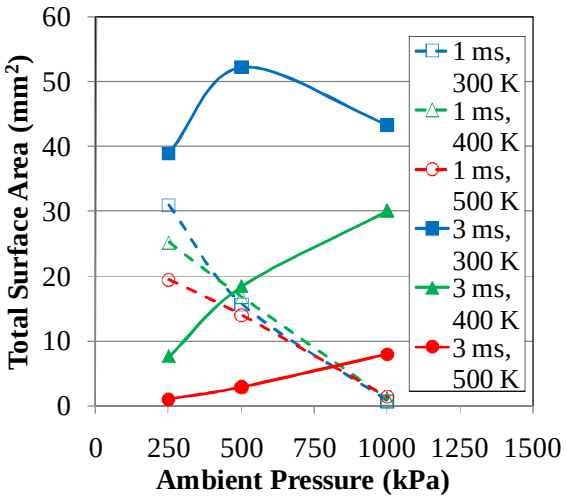

Figure 3. Total surface area as a function of ambient pressure. P_{fuel} = 10 MPa, T_{fuel} = 90° C.

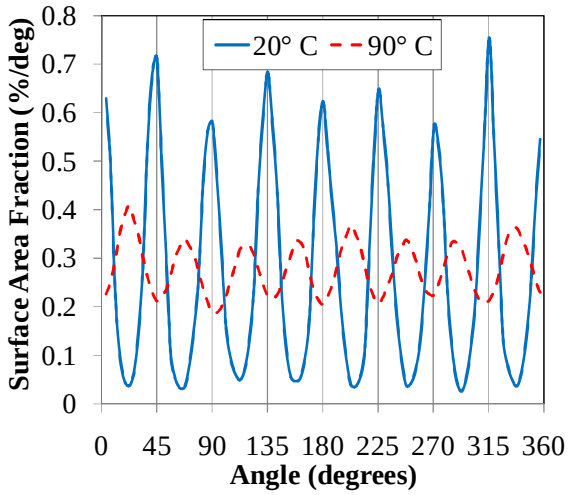

Figure 4. Surface area fraction as a function of angle for two fuel temperatures. P_{fuel} = 10 MPa, $P_{ambient}$ = 40kPa, $T_{ambient}$ = 300°K, 1 ms period.

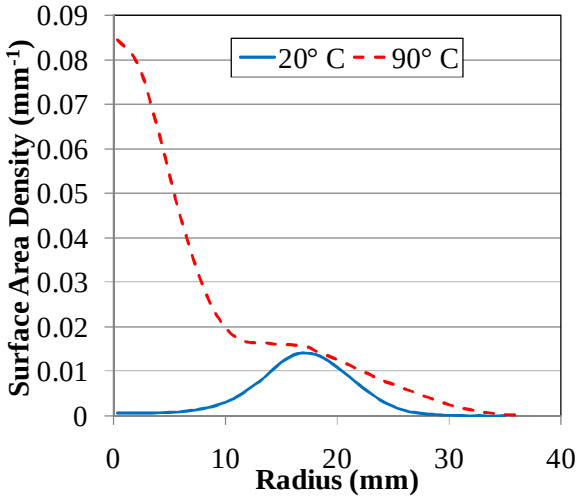

Figure 5. Mean surface area density as a function of radius for two fuel temperatures. P_{fuel} = 10 MPa, $P_{ambient}$ = 40kPa, $T_{ambient}$ = 300° K, 2 ms period.

Influence of Fuel Temperature at Low Ambient Pressure – By comparing the spray patterns of the 20° C fuel temperature to the 90° C fuel temperature at ambient pressures less than atmospheric pressure, in both Figure A.1 and A.4, it can be seen that fuel temperature has a substantial impact on the spray pattern at low ambient pressure. In fact, at the lowest ambient pressure, 40 kPa, individual plumes are no longer discernable for the 90° C fuel temperature. The combination of low ambient pressure and high fuel temperature results in the fluid reaching a superheated state and promotes rapid phase change during the injection event. This phenomenon is commonly referred to as flash boiling. In the case of the 10 MPa fuel pressure, as indicated in the 1 ms frame, the plumes have expanded to such a degree that adjacent plumes have impinged upon one another to form "plumes" between plumes. This effect is further illustrated in Figure 4 where surface area fraction at various radii is plotted as a function of radii angle. In the 20° C fuel temperature case, eight peaks in surface area fraction, each corresponding to a spray plume, are easily identified. Likewise, in the 90° C fuel temperature case, eight peaks are identifiable but their locations are between those of the 20° C fuel temperature case.

The 2 ms frames exhibit high concentrations of surface area at the center of the pattern indicating a "collapsed" spray structure. This can be quantified by calculating the mean surface area density verses radial location in the spray pattern as shown in Figure 5. For the 20° C fuel case, the peak surface area density occurs at a radius near 17 mm and there is a very low surface area density at the center of the pattern. In contrast, for the 90° C fuel temperature case, the peak surface area density occurs at the center of the pattern. These finding corroborate other work that investigated the same conditions with a different diagnostic [11].

Influence of Fuel Temperature at High Ambient Pressure – The influence of fuel temperature on spray patterns at ambient pressures greater than atmospheric pressure is quite subtle in comparison to the influence at low ambient pressure. The only appreciable difference when comparing the spray patterns of one fuel temperature to the other at corresponding conditions is the reduction in surface area density associated with the 90° C fuel temperature. This is most evident at the 400° K and 500° K ambient temperatures. This reduction is due to enhanced vaporization promoted by the higher fuel temperature.

Influence of Ambient Temperature - By comparing corresponding spray patterns at different ambient temperatures, it is apparent that although the spray pattern

remains fairly consistent, the surface area diminishes as ambient temperature increases. This is particularly evident when comparing the 3 ms frames. At an ambient temperature of 300° K most of the 3 ms spray patterns exhibit a multiple plume structure. In contrast, at 500° K the 3 ms patterns do not exhibit a recognizable structure and in some cases little or no surface area is detected. The total surface areas for the 3 ms frames for the 10 MPa injection pressure and 90° C fuel temperature are shown in Figure 3. This behavior is due to both a reduction in particle size and number due to fuel vaporization.

Influence of Injection Pressure - In general when comparing corresponding conditions, the spray patterns associated with the 20 MPa fuel pressure are slightly larger than those of the 10 MPa fuel pressure. In addition, the size of the individual spray plumes are larger for the 20 MPa fuel pressure. These observations indicate, as expected, that radial penetration increases with injection pressure. Comparing corresponding 1 ms frames, it is also apparent that the strength of the 20 MPa spray patterns are greater than those of the 10 MPa injection pressure indicating an increase in axial penetration.

Spray Angles – Acquiring measurements in two planes enables the calculation of spray angles. The calculation is straightforward and essentially requires that an equivalent diameter be determined for each plane. Figure 6 shows the results of spray angle measurements as a function of ambient pressure for the 300° K ambient temperature cases. As opposed to using just one of the time periods, the average of all three time periods was used to determine a time averaged spray angle. Identification of the edge of the spray was accomplished by finding the radial location where the surface area density was equal to 10 percent of the maximum surface area density. The trends were similar for each case. The largest spray angles were found to occur at the lowest ambient pressure. Initially, as ambient pressure is increased spray angles become smaller. This behavior is due to reduced radial penetration as ambient pressure increases. At ambient pressures between 120 kPa and 250 kPa, the spray angles begin to become larger as ambient pressure is further increased. This reversal in behavior is likely related to the interaction of the spray with the surrounding high density gas. This interaction typically causes toroidal vortex structures to form on the periphery of the spray. These structures lead to an apparent increase in spray width resulting in larger spray angles. The trend of increasing spray angle with ambient pressure continues through the 500 kPa ambient pressure. At 1000 kPa ambient pressure, spray angles reduce in comparison to the 500 kPa ambient pressure. This is likely due to an excessive loss of penetration. In the 20° C fuel temperature cases, the spray angles of the 20 MPa fuel pressure are approximately 10 degrees larger, on average, than those of the 10 MPa injection pressure. This is due to an increase in radial penetration and stronger interaction with the surrounding gas. In general, the 90° C fuel temperature cases exhibit larger spray angles than the corresponding 20° C fuel temperature cases. This is particularly evident at ambient pressures less than atmospheric pressure where flash boiling effects promote expansion of the spray pattern.

It should be noted that some of spray angle trends observed in this work may be dependant on the locations where the measurements were performed. For example, if measurements were performed closer to the tip of the injector where toroidal vortex structures are not present spray angle trends may be different from those found in this work.

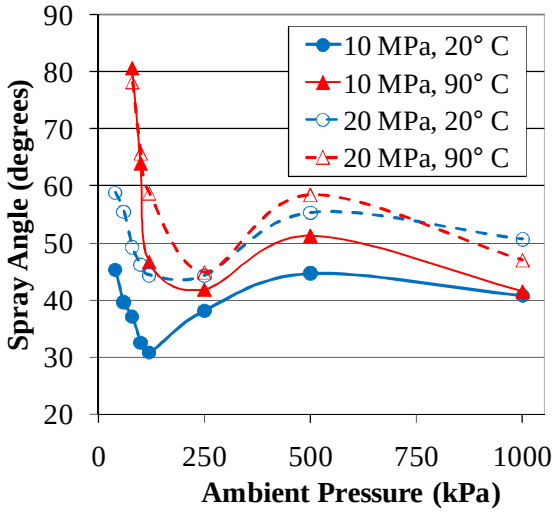

Figure 6. Spray angle as a function of ambient pressure. $T_{ambient}$ = 300° K, Average of all time periods.

Summary and Conclusions

Planar line-of-sight extinction tomography measurements were performed to evaluate an 8-hole, VCO style injector to determine the influence of ambient pressure and temperature and fuel pressure and temperature on spray structure. For the operation conditions investigated, the following can be concluded:

- Under flash boiling conditions, sprays tend to collapse and change shape significantly. Individual spray plumes can expand to such a degree that they impinge upon one another to form “plumes” between plumes.
- For ambient pressures greater than one atmosphere, spray patterns appear similar for the 90° C and 20° C fuel temperatures. Surface area densities are lower for the 90° C fuel temperature compared to the 20° C fuel temperature, particularly at high ambient temperatures.

- As ambient temperature increases, surface area diminishes significantly but spray patterns remain similar.
- In the 300° K ambient temperature cases, spray angles were found to initially become smaller, then larger, and finally once again smaller, with increasing ambient pressure.
- For the 300° K ambient temperature with 20° C fuel temperature case, spray angles were found to be approximately 10 degrees larger for the 20 MPa fuel pressure compared to the 10 MPa fuel pressure.

Line-of-sight extinction tomography was found to be an effective tool for characterizing dense, high velocity, transient sprays.

References

1. Zhao, F., Harrington, D. L., and Lai, M-C., *Automotive Gasoline Direct-Injection Engines*, SAE International, ISBN Number**:** 978-0-7680-0882-1, 2002, pp. 51-116.
2. Spiegel, L., and Spicher, U., "Mixture Formation and Combustion in a Spark Ignition Engine with Direct Fuel Injection," SAE 930521.
3. Park, S.W., Kim, H.J, and Lee, C.S., "An Experimental and Numerical Study on Atomization Characteristics of Gasoline Injector for Direct Injection Engines," *15th Annual Conference on Liquid Atomization and Spray Systems*, Madison, WI, May 2002.
4. Parrish, S.E., and Farrell, P.V., "Transient spray characteristics of a direct-injection spark-ignited fuel injector," SAE 970629.
5. Dahlander, P., and Denbratt, I., "Experimental investigation of fuel pressure influence on droplet size and velocity for a gasoline multi-hole direct injection injector spray under vaporizing conditions in a constant pressure chamber," *18th Annual Conference on Liquid Atomization and Spray Systems*, Irvine, Ca, May 2005.
6. Schmitz, I., Ipp, W., and Leipertz, A., "Flash Boiling Effects on the Development of Gasoline Direct-Injection Engine Sprays," SAE 2002-01-2661.
7. VanDerWege, B. A., and Hochgreb, S., "Effects of Fuel Volatility and Operating Conditions on Fuel Sprays in DISI Engines: (1) Imaging Investigation," SAE 2000-01-0535.
8. Davy, M. H., Williams, P. A., and Anderson, R. W., "Effects of Fuel Composition on Mixture Formation in a Firing Direct-Injection Spark-Ignition (DISI) Engine," SAE 2000-01-1904.
9. Marriott, C. D., Wiles, M. A., Gwidt, J. M., and Parrish, S.E., "Development of a Naturally Aspirated Spark Ignition Direct-Injection Flex-Fuel Engine," SAE 2008-01-0319.
10. Parrish, S.E., and Zink, R.J., "Spray characteristics of multi-hole injectors under flash boiling conditions," *21st Annual Conference on Liquid Atomization and Spray Systems*, Orlando, Florida, May, 2008.
11. Lim, J., Sivathanu, Y., Narayanan, V., and Chang, S., "Optical Patternation of a Water Spray using Statistical Extinction Tomography," Atomization and Sprays, Vol. 13, pp. 27-43, 2003.
12. Lim, J., and Sivathanu, Y., "Optical Patternation of a Multi-Orifice Spray Nozzle," Atomization and Sprays, Vol. 15, pp. 687-698, 2005.

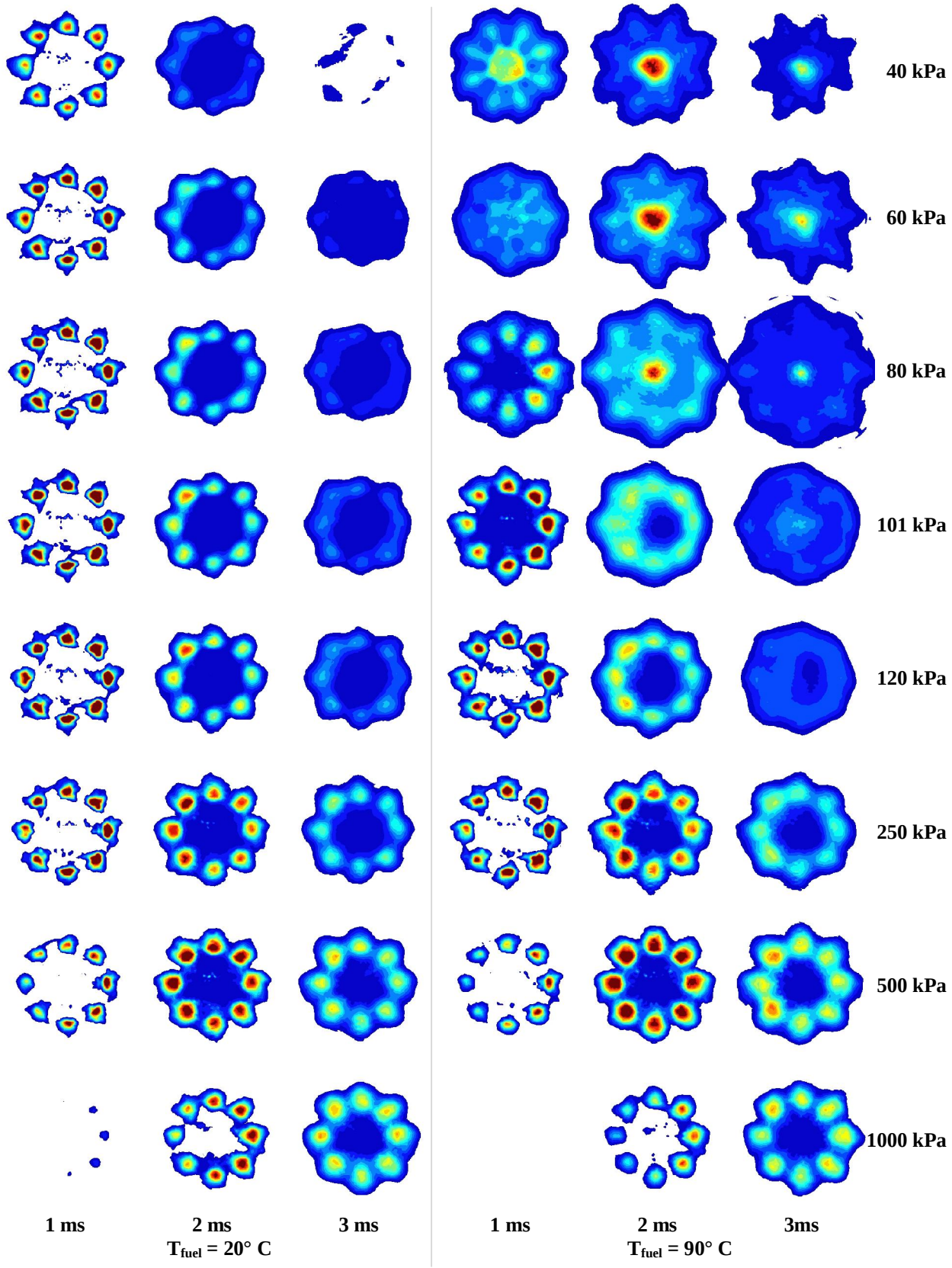

Figure A.1 Spray patterns at various ambient pressures. 40 mm plane, P_{fuel} = 10 MPa, $T_{ambient}$ = 300° K

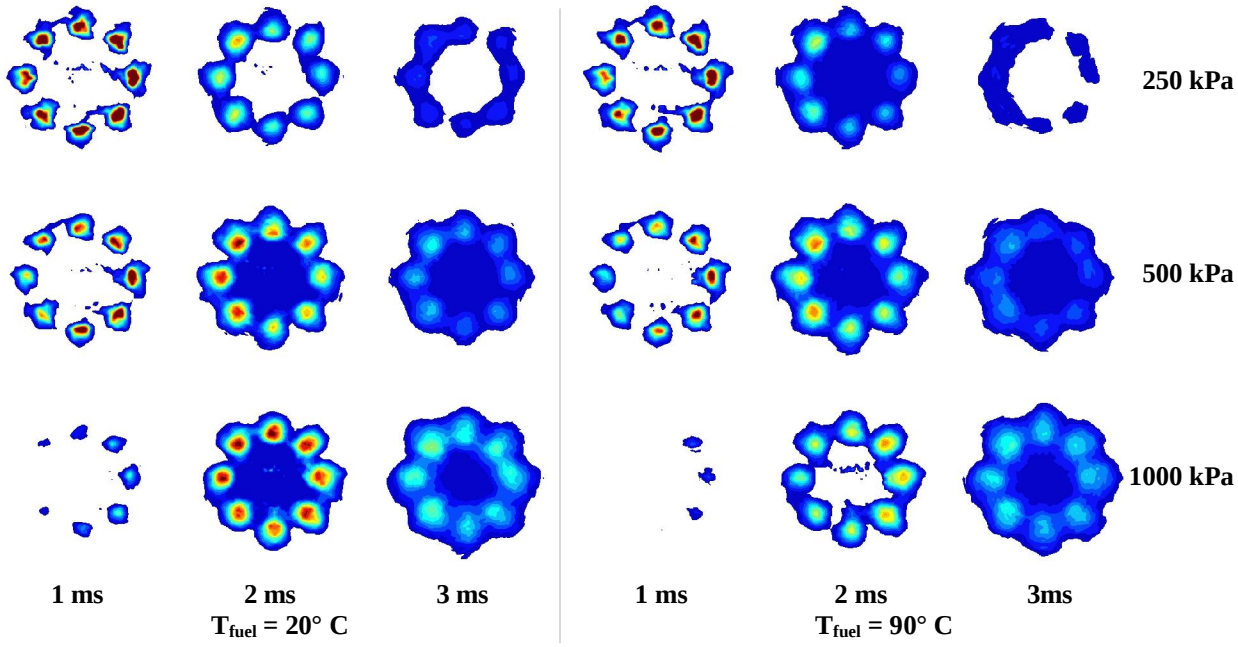

Figure A.2 Spray patterns at various ambient pressures. 40 mm plane, P_{fuel} = 10 MPa, $T_{ambient}$ = 400° K

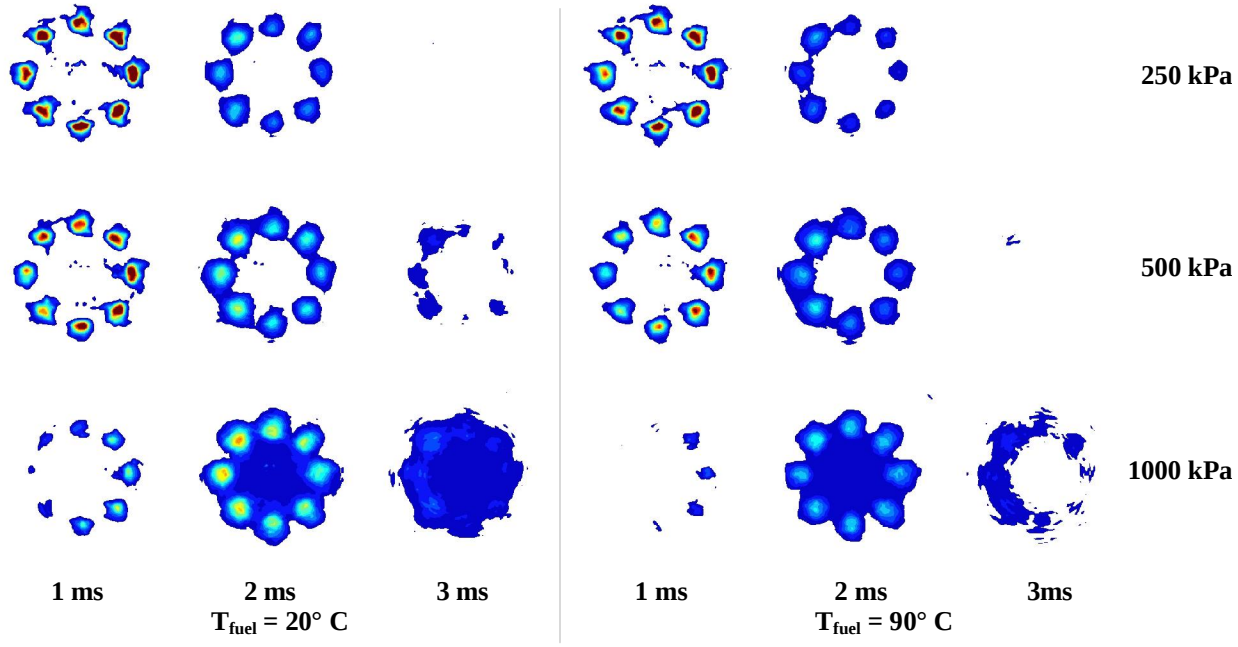

Figure A.3 Spray patterns at various ambient pressures. 40 mm plane, P_{fuel} = 10 MPa, $T_{ambient}$ = 500° K

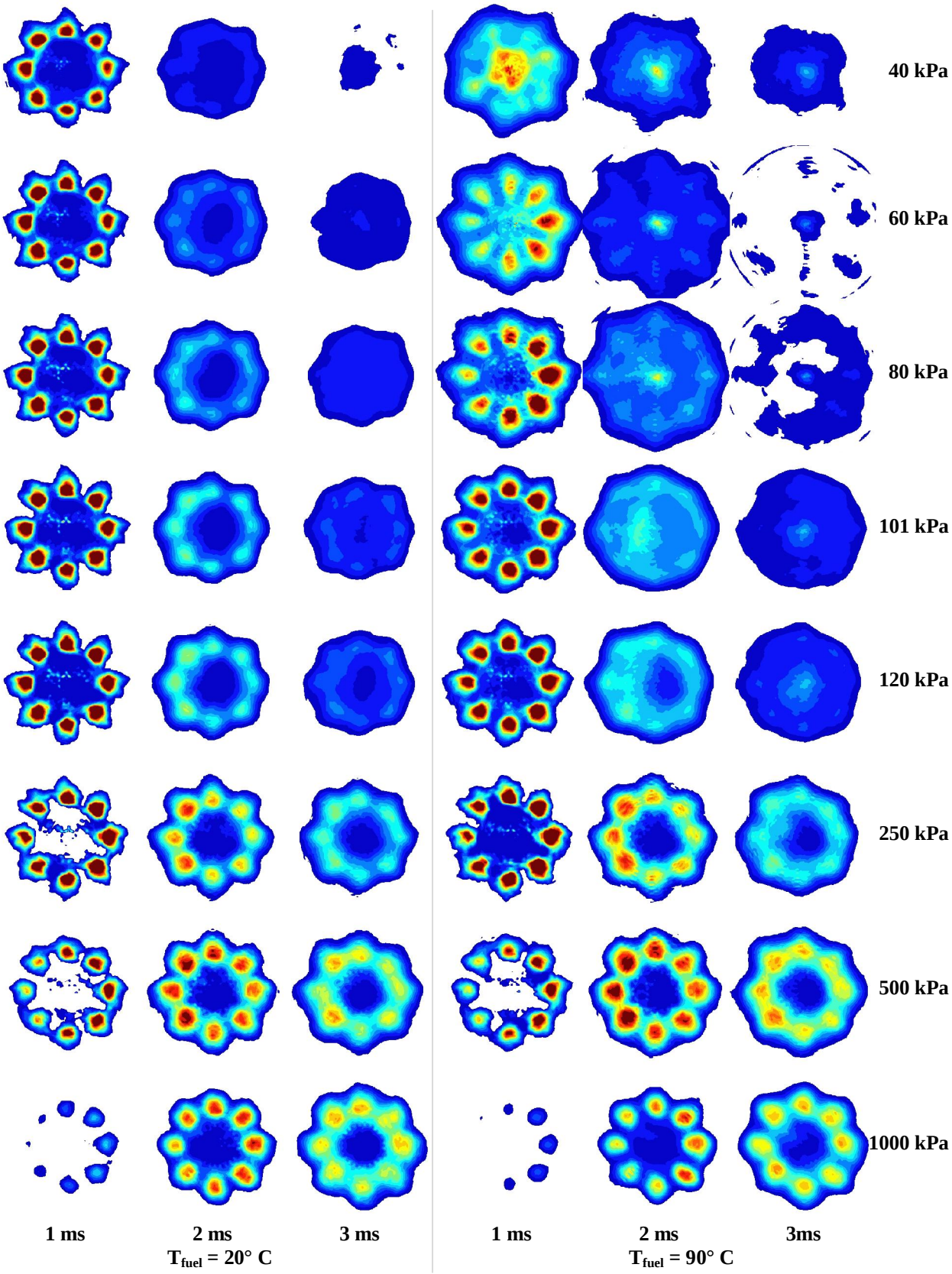

Figure A.4 Spray patterns at various ambient pressures. 40 mm plane, P_{fuel} = 20 MPa, $T_{ambient}$ = 300° K

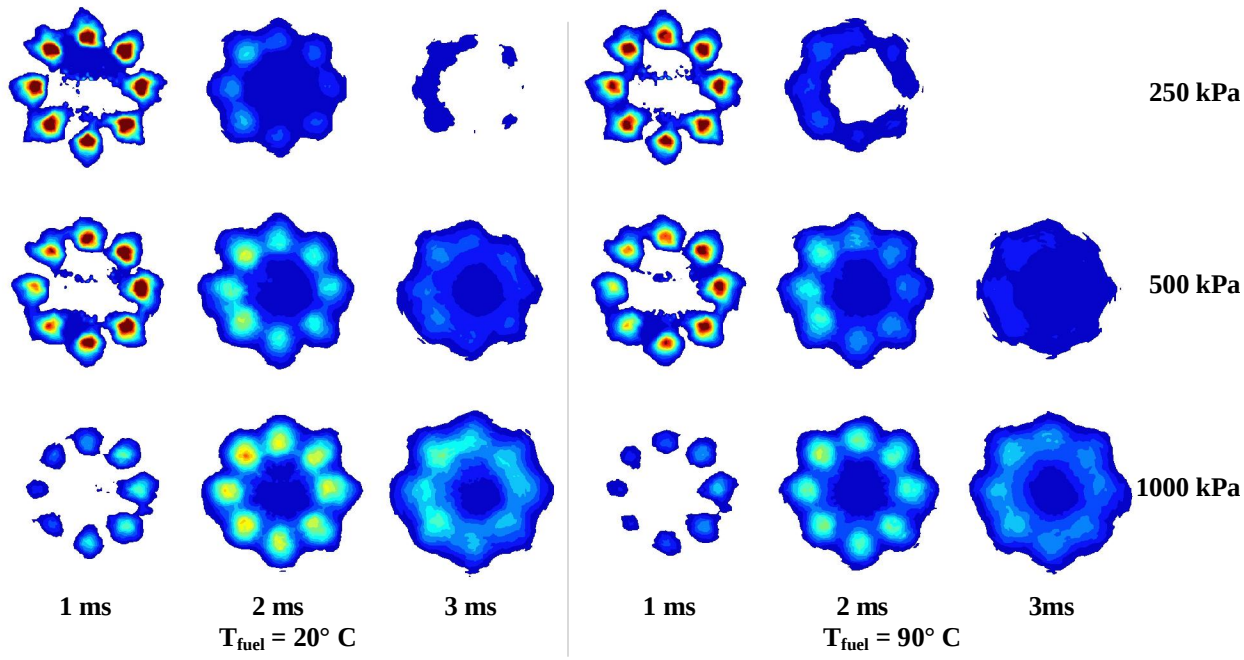

Figure A.5 Spray patterns at various ambient pressures. 40 mm plane, P_{fuel} = 20 MPa, $T_{ambient}$ = 400° K

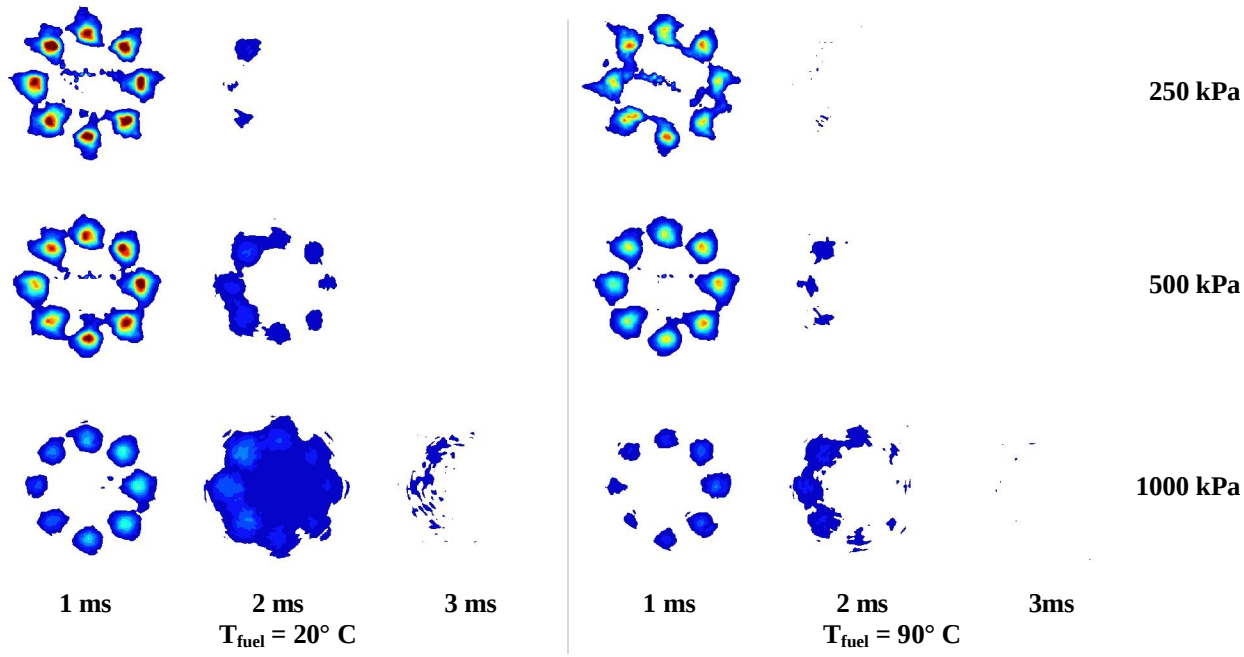

Figure A.6 Spray patterns at various ambient pressures. 40 mm plane, P_{fuel} = 20 MPa, $T_{ambient}$ = 500° K